High-Temperature Lightweight Ceramics with Nano-sized Ferrites for EMI Shielding: Synthesis, Characterization, and Potential Applications

Vitalijs Abramovskis , Ilmars Zalite , Mikhail Maiorov , Janis Baronins , Ashish Kumar Singh , Vjaceslavs Lapkovskis , Saurav Goel , Andrei Shishkin *

Posted Date: 2 November 2023

doi: 10.20944/preprints202311.0173.v1

Keywords: cenospheres; CoFe2O4; high-temperature sintering; magnetic properties; syntactic foam

Article

High-Temperature Lightweight Ceramics with Nano-sized Ferrites for EMI Shielding: Synthesis, Characterization, and Potential Applications

Vitalijs Abramovskis [1], Ilmars Zalite [2], Mikhail Maiorov [3] Janis Baronins [1], Ashish Kumar Singh [4], Vjaceslavs Lapkovskis [1], Saurav Goel [5] and Andrei Shishkin [1,*]

[1] Laboratory of ecological solutions and sustainable development of materials, Institute of General Chemical Engineering, Faculty of Materials Science and Applied Chemistry at Riga Technical University, Pulka 3, K-3, Riga, LV-1007, Latvia; andrejs.siskins@rtu.lv (A.S.), vitalijs.abramovskis@edu.rtu.lv (V.A.), janis.baronins@rtu.lv (J.B.)

[2] Institute of Materials and Surface Technologies of the Riga Technical University, P. Valdena iela 7, Riga, LV-1048, Latvia; ilmars.zalite@rtu.lv (I.Z.)

[3] Institute of Physics of University of Latvia, Miera iela 32, Salaspils, LV2169, Latvia; maiorov@sal.lv (M.M.)

[4] SMW Group AS, Kr. Barona Street 3-1, Riga, Latvia, LV-1050; aksingh@smw.com (A.K.)

[5] School of Engineering, London South Bank University, London, SE1 0 AA, UK goels@lsbu.ac.uk (S.G)

* Correspondence: andrejs.siskins@rtu.lv

Abstract: Present study focuses on the synthesis and characterisation of a lightweight ceramic material with electromagnetic interference (EMI) shielding properties, achieved using mullite containing micrometer-sized hollow spheres (cenospheres) and $CoFe_2O_4$ nanoparticles. The research explores compositions with varying $CoFe_2O_4$ content, ranging from 0 up to 20 wt.%. Conventional sintering in an air atmosphere is carried out at a temperature between 1100-1300 °C. The addition of ferrite nanoparticles was found to enhance the sintering process of cenospheres, resulting in improved material density and mechanical properties. Furthermore, the study reveals a direct correlation between the concentration of ferrite nanoparticles and the electromagnetic properties of the. By increasing the concentration of ferrite nanoparticles, the electromagnetic shielding effect of the material (saturation magnetization (Ms) and remanent magnetization (Mr)) was observed to strengthen. These findings provide valuable insights into the design and development of lightweight ceramic materials with enhanced electromagnetic shielding capabilities. The synthesized ceramic material holds promise for various applications that require effective electromagnetic shielding, such as in electronics, telecommunications, and aerospace industries.

Keywords: cenospheres; $CoFe_2O_4$; high-temperature sintering; magnetic properties; syntactic foam

1. Introduction

Radiation fields from electronic devices like antennas, phones, and household appliances cause electromagnetic interference (EMI). Shielding sensitive electronics from EMI is challenging for aircraft, military, and communication system components [1]. Efforts to combat EMI involve developing shielding systems for intentional or unintentional interference. However, using metallic materials for EMI shielding is becoming difficult due to the trend toward smaller and lighter electronic packaging [2].

Industry traditionally use electrically conductive metals for EMI shielding, but their high density and susceptibility to corrosion lead to heavyweight shielding components. To address this, researchers have turned to low density materials like polymers, which have poor electrical conductivity and EMI shielding. Two approaches are used to prepare polymer shields: coating with conductive metals or blending with conductive fibers and particles [3]. Researchers have attempted to reinforce transparent polymers with conductive fillers like carbon nanofibers [4,5], carbon nanotubes [6], graphene [7,8], and metallic nanowires and particles [9,10]. Syntactic foams are

 doi:10.20944/preprints202311.0173.v1

lightweight composite materials with hollow particles dispersed in a polymer matrix that offer weight-saving potential and are being explored for their EMI shielding effectiveness [11].

The development of lightweight and mechanically robust porous or cellular materials is one of the current trends in modern materials design. In recent years, the use of cenospheres (CS) for manufacturing porous lightweight composite materials has been extensively investigated. CS is three-dimensional objects with a spherical shape that contains a cavity or empty spaces inside. These materials are chemically multicomponent systems with SiO_2-Al_2O_3-Fe_2O_3 content of about 90 wt.% [12–14]. Due to their low apparent density (0.40-0.72 $g \cdot cm^{-3}$), low thermal conductivity (about 0.065 $W \cdot m^{-1} \cdot K^{-1}$), and excellent stability in alkaline solutions and at high temperatures, cenospheres are a promising raw material for the development of new porous materials. The particle size of cenospheres ranges from about 40 up to 500 μm [15,16].

The civil engineering industry widely applies CS in producing lightweight concrete with improved thermal insulation [14,17]. CS also takes filler and reinforcement roles in metal-matrix [18–20] and polymer-matrix [20,21] composites. However, researchers rarely report results of CS containing low-density ceramic-matrix composites. However, interest in ceramic-cement composites has gained in recent years, and researchers have reported some stunning results.

CS exhibit reliable sintering tendencies while maintaining their spherical shape, yet they do not possess the ability to form durable structures. Therefore, adding a second phase, which promotes the adhesion of the material, can improve its mechanical strength. In addition, various additives can promote sintering, e.g., metals, oxides, or other additives. For example, one way to enhance sintering could be using oxides, e.g., ferrite nanoparticles [22].

Cobalt ferrite ($CoFe_2O_4$) has excellent chemical stability, mechanical hardness, and electrical insulation. On the other hand, it is a hard magnetic material, and its magnetic properties exhibit size dependence. Therefore, using $CoFe_2O_4$ nanoparticles (NP) in composite production could have a positive effect. In addition, the spinel structure of $CoFe_2O_4$ allows the introduction of different metallic ions into its lattice, thus altering the structural, magnetic, electrical, and catalytic properties [23]. It has many applications, such as magnetic data storage, hybrid electric vehicles, transformer core, high-frequency integrated inductors, biocompatible magnetic fluids, magnetic resonance imaging, and controlled drug delivery. Other industries also implement $CoFe_2O_4$ in manufacturing microwave-absorbing paints, catalysis, hybrid supercapacitors, and products of different applications [24,25]. The remarkable magnetic properties, such as high coercivity (H_C), magneto crystalline anisotropy constant (K), Curie temperature (T_C), moderate saturation magnetization (M_S) and remanent magnetization (Mr), high magnetostriction coefficient (λ), and low eddy current losses, along with excellent chemical and mechanical stability, electrical resistance, optical and dielectric properties, low toxicity [26–29], and impressive mechanical hardness, present $CoFe_2O_4$, as a good candidate for producing syntactic foams with $CoFe_2O_4$.

$CoFe_2O_4$ nanoparticles have been used as standalone materials and incorporated with other materials, such as polymers and carbon-based materials, to improve their magnetic properties. There is significant literature describing the various material design methods and applications of these materials, including EMI shielding, catalysts, and magnetism-related applications [30–37]. Spinel $CoFe_2O_4$ prepared by sol-gel assisted sintering at 1150 °C by Caldeira et. al. [38], exhibited Vicker's hardness of 133.9. Hollow $CoFe_2O_4$ spheres on carbon template have been prepared for high wave absorption by Zhou et. al. [39]. A porous lightweight nano composite of $CoFe_2O_4$ and graphene oxide was prepared by Liu et. al. [40] that displayed high microwave absorption [23].

For use in real-life EMI shielding applications, it is necessary that the material has sufficient mechanical strength and low density. In the aerospace industry has additional requirements to the materials - is to withstand high-temperatures (up to 1000 °C). But most of the EMI shielding materials mainly made of (or contain) polymer materials [41] which decomposes at 250-350 °C, or contain graphite or graphene [41] which burn out at 350-450 °C.

In this study, the preliminary investigation into the formability and structural integrity of a novel CS-$CoFe_2O_4$ composite foam has been conducted. With the incorporation of $CoFe_2O_4$ nanoparticles in CS matrix, a lightweight, high-temperature ceramic material capable of electromagnetic wave

Preprints (www.preprints.org) | NOT PEER-REVIEWED | Posted: 2 November 2023 doi:10.20944/preprints202311.0173.v1

absorption can be produced. Generally, a high-performance absorber must possess strong absorptivity, low density, broad absorption frequency, and thin thickness to satisfy the requirements of actual applications [42–44]. The effect of sintering temperature and Compaction Pressure (CP) on the mechanical properties is investigated. This article also demonstrates the effect of $CoFe_2O_4$ nanoparticles as an additive for the sintering of CS while improving magnetic properties [24,25]. The authors studied two ceramic types: pure CS and CS-based ceramics with $CoFe_2O_4$ addition. The following characterisation methods, materials, and sintering approach demonstrate the effect of applied compressive pressure, sintering temperature, and the amount of added ferrite on the density and properties of ceramics. This paper investigates and discusses material mechanical strength, porosity and density. Based on these observations, the recipe with the best properties combination will be used in further EMI absorber design and study.

2. Materials and Methods

2.1. Materials

The authors selected mullite-based CS (Biotecha SIA, Latvia) [15] with two different particle size distributions, 63 – 150 μm (CS2) and 150 – 250 μm (CS1). An optical image and the representative XRD spectrum of as received CS2 is shown in **Figure 1**a and 1b, respectively. The authors have provided a more detailed description of selected CS properties in one of their previous publications [15]. The mullite-based CS exhibit exceptional mineral mechanical strength and chemical corrosion resistance. Their robustness makes them ideal for applications requiring durability and resilience in high-temperature and corrosive environments. The specific sintering temperature and pressure required to maintain the hollow nature of mullite-based CS while sintering them into a single object can vary depending on various factors, including the composition of the cenospheres and the desired final properties. However, in general, a typical sintering temperature range for mullite-based CS is around 1200 to 1600 °C. The pressure applied during the sintering process can vary but is often conducted under atmospheric pressure or in a low-pressure environment to avoid collapsing the hollow structure.

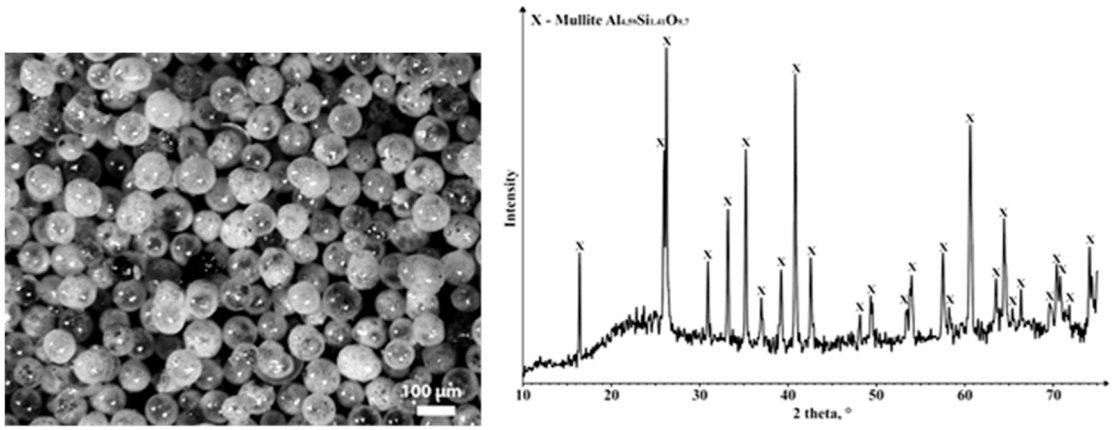

(a) **(b)**

Figure 1. Images of (a) CS2 sample obtained (optical microscope) and (b) phase composition of mullite containing cenospheres with diameters from 63 up to 100 μm (sample CS1 exhibit similar result).

$CoFe_2O_4$ nano powder with an average particle size of 40 nm was prepared by high-frequency plasma chemical synthesis [45]. This process produced nanoparticles of different sizes (Figure 2a) and their XRD spectrum (Figure 2b) matches the peaks of $CoFe_2O_4$ obtained using the chemical co-precipitation method [46].

Preprints (www.preprints.org) | NOT PEER-REVIEWED | Posted: 2 November 2023 doi:10.20944/preprints202311.0173.v1

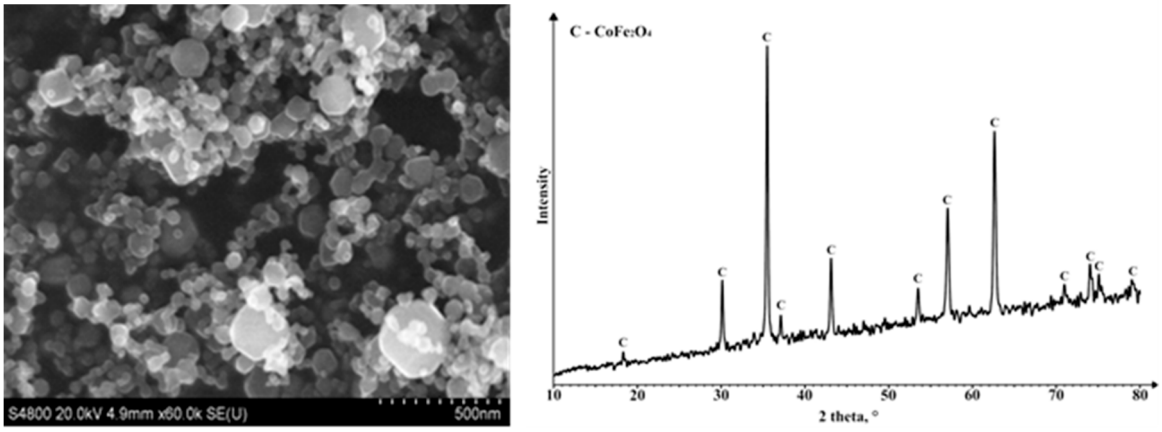

(a) **(b)**

Figure 2. Images of (a) $CoFe_2O_4$ nanoparticles obtained by plasma chemical synthesis (SEM) and (b) phase composition $CoFe_2O_4$ nano powder (d_{50}= 40 nm).

These nanoparticles can be sintered completely at 1100-1200 °C [47], forming a compacted material. The electromagnetic properties of pure $CoFe_2O_4$ material are shown in **Figure 3**. A small additive of nanoparticles can create a connective network between the cenospheres, improving the strength of the structure. The ceramic engineer made compositions with $CoFe_2O_4$ content from 0 to 20 wt.%. Therefore, the authors expect the lowered required sintering temperature to produce CS-based ceramic materials with $CoFe_2O_4$ nanoparticle additives [15].

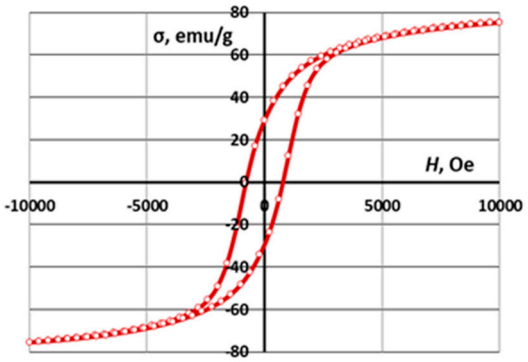

Figure 3. Magnetic properties of ferrites $CoFe_2O_4$ synthesized in plasma.

Table 1. Magnetic properties of $CoFe_2O_4$.

	Magnetic properties		
Ferrite	**Ms, emu/g**	**Mr, emu/g**	**Hc, Oe**
$CoFe_2O_4$	75.4	32.0	780

2.2. Sintering process

The flowchart of the methodology used for the research is shown in **Figure 4**. Sintering was performed at 1100–1300 °C in an LHT-08/18 furnace (Nabertherm GmbH) in an air atmosphere with a heating rate of 10 °C·min^{-1} and a residence time at the maximum temperature of 1h. The CP of the samples was 25-125 bar. Cylindrical sample size ⌀=12 mm and h=10 mm. Samples with dimensions of 65 x 65 x 9 mm were made for determining the mechanical properties.

Preprints (www.preprints.org) | NOT PEER-REVIEWED | Posted: 2 November 2023 doi:10.20944/preprints202311.0173.v1

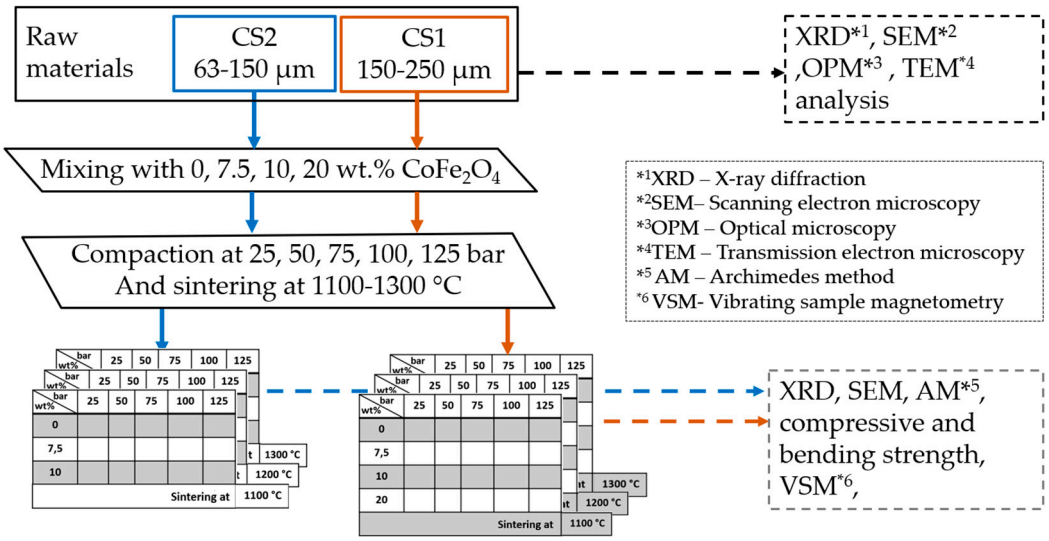

Figure 4. Flowchart of receiving and researching $CoFe_2O_4$ composite material.

2.3. Applied Characterization Methods

An operator employed an Advance D8, Bruker AXS X-ray diffraction (XRD) analysis system with Cu-Ka radiation, utilising the ICDD database PDF-4 + 2008, PDF-4/Organics 2008, and Sleve+2008 software, to characterise the phase composition of raw materials and sintering products. An operator used Hitachi S4800 and Mira/Tescan scanning electron microscopes (SEM) to evaluate the morphology and microstructure of CS and produced ceramic composites. In addition, researchers conducted optical imaging using a Keyence VHX-2000 digital optical microscope equipped with VH-Z20R/W and VH-Z500R/W lenses.

Furthermore, the TEM JEM-100S "JEOL" was employed to analyse the nanoparticle microstructure. The laboratory assistant used the Archimedes method to determine the bulk density, apparent porosity, water absorption, and apparent specific gravity of the sintered samples. The technician conducted compressive and bending strength tests using the ToniNorm Tinius Olsen 25ST apparatus. The magnetic properties of the manufactured materials were analysed using vibrating sample magnetometry (VSM) with Lake Shore Cryotronics Inc., model 7404 VSM.

Apparent density and porosity were determined by the Archimedes method at 20 °C, using a distilled water as liquid media for immersing.

3. Results and Discussion

Most of the studies have been carried out using cenospheres CS1 with sphere size in the range of 150-250 µm ((Figures 7, 8, 10, 12, 13), as well as using cenosphere CS2 (Figures 5, 9, 11). The results show that as the sintering temperature increases, the density of the material increases due to decrease in the content of moisture and apparent porosity by consolidation of material. Similar trend was observed with increasing CP used for producing of samples. In all sintering modes, regardless of the size of the ferrite nanoparticle additive, as the CP of the samples increases, the density of the material increases, and apparent porosity of the material decreases. Density of a cellular material has a positive impact on its mechanical response. Similar relationship between density and compressive strength was observed in this study as well. Various concentrations of ferrites were used in the composite material: 0 wt. % (CS1-0, CS2-0), 7.5 wt. % (CS1-7.5 and CS2-7.5), 10 wt. % (CS1-10, CS2-10) and 20 wt. % (CS1-20). In all these variants, it was seen that as the concentration of ferrite nanoparticles increases, the density of the material increases, irrespective of the sintering temperature. With increasing density (decreasing porosity) the compressive strength of the materials also increases.

For the range of sintering parameters used in the study (p = 50 bar to 125 bar, t = 1100 °C to 1300 °C, $CoFe_2O_4$ content from 0 to 20 wt.%), samples with density of 1.19-2.16 $g \cdot cm^{-3}$ and a compressive strength of 1.5 – 125 MPa were obtained.

Preprints (www.preprints.org) | NOT PEER-REVIEWED | Posted: 2 November 2023 doi:10.20944/preprints202311.0173.v1

Composition CS2-0 (without $CoFe_2O_4$) sintered at 1100 °C and compacted at all studied CP range (25-125 Bar), has very low strength (below 1 MPa) (**Figure 5**).

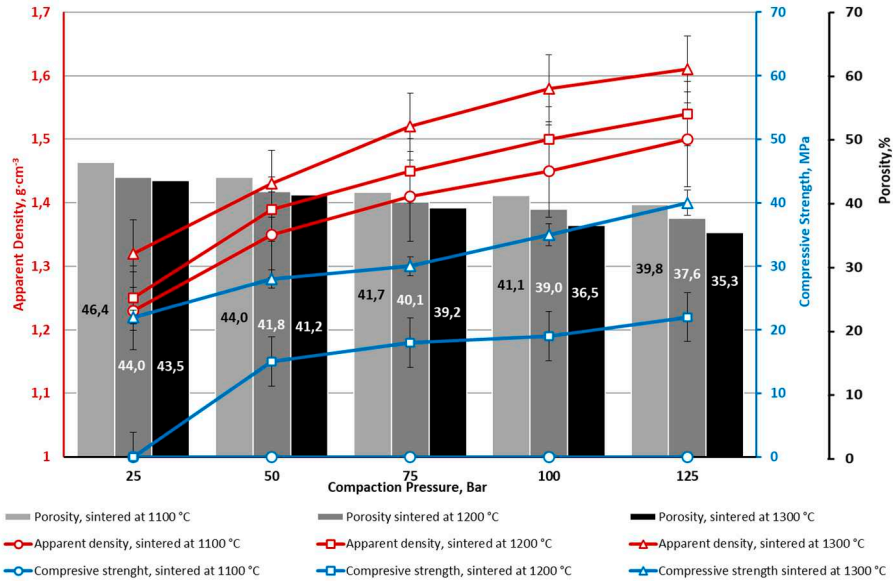

Figure 5. Ceramics apparent density, apparent porosity and compressive strength depending on CP and sintering temperature CS2-0.

This fact could be explained by low CS particles adhesion to each other due to low (1100 °C) temperature. As described in previous research [15], this type of CS has good thermal stability (no softening, no shrinkage below 1250 °C. This is clearly seen on the **Figure 6**, where is seen area's cross section decrease of CS1, started from 1250 °C.

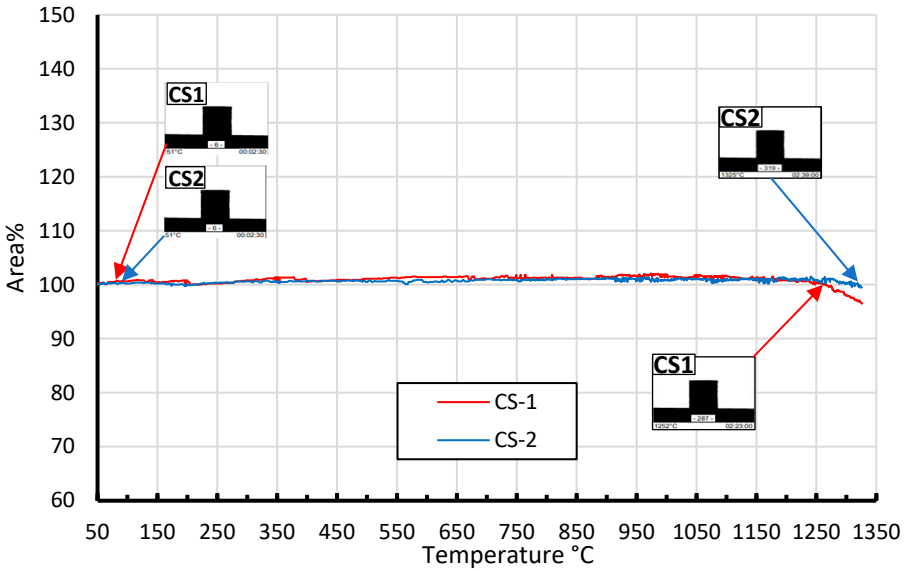

Figure 6. CS1 and CS2 high-temperature optical dilatometry curves in the 50-1325 °C temperatures interval, adopted from [15]. Reprint on CC BY, 4.0 Open Access licence from [15].

The same weak particles adhesion to each other noticed for specimens sintered at 1200 °C and CP 25 bar. At the same time, other specimens series: sintered at 1300 °C (CP=25 ÷ 125 bar), and at 1200 °C, (by except CP=25 bar) demonstrate significant enough mechanical strength. As can be seen on Figure 5, increasing sintering temperature from 1100 to 1200 °C, in average compressive strength

Preprints (www.preprints.org) | NOT PEER-REVIEWED | Posted: 2 November 2023 doi:10.20944/preprints202311.0173.v1

increase for 20 MPa. It is interesting to note that density of the CS2-0 sintered materials increase gradually (and porosity has reverse dependence, which is logically, but also gradually) in all studied sintering temperatures and CP. The mechanical properties increases drastically by increasing the sintering temperature from 1100 to 1200 and to 1300 °C - average increase for 20 MPa per 100 °C. This is could be explained by CS softening, as result a better compaction, what also supported by high-temperature optical dilatometry curves (Figure 6). But CP brings a much smaller contribution into mechanical properties for the samples CS2-0, comparing with the sintering temperature: 2-3 MPa for 1200 °C and 3-6 MPa for 1300 °C.

Composition CS1-0 demonstrate quite similar dependences, but demonstrate slightly higher compression strength of series sintered at 1100 °C, than the same series of CS2-0. Sintered at 1100 °C and compacted at all studied CP range (25-125 bar), has very low strength (below 3 MPa) (**Figure 7**). The same weak particles adhesion to each other noticed for specimens sintered at 1200 °C and CP 25 bar. At the same time, other specimens series: sintered at 1300 °C (CP=25 ÷ 125 bar), and at 1200 °C, (by except CP=25 bar) demonstrate significant enough mechanical strength.

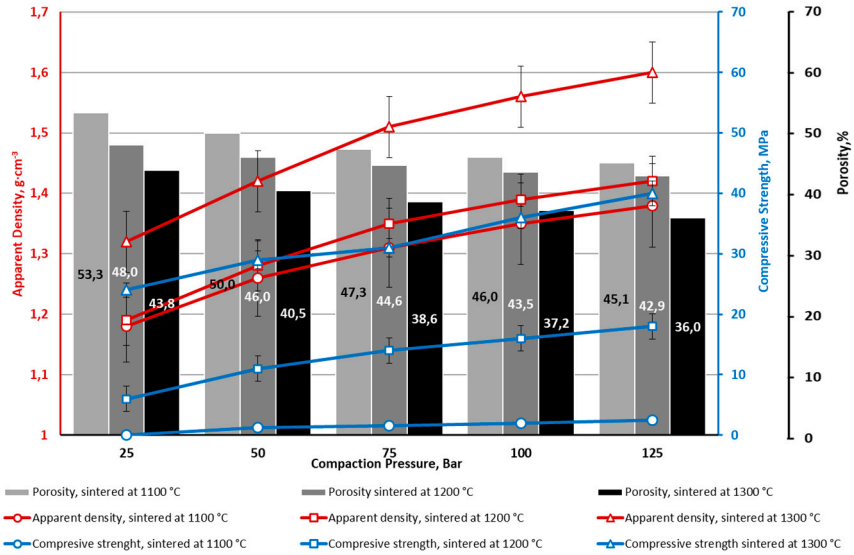

Figure 7. Ceramic apparent density, apparent porosity and compressive strength depending on CP and sintering temperature for CS1-0.

Series with $CoFe_2O_4$ has lower porosity's value for average 10% (for CS1) and 7% (for CS2) (Figures 8 and 9). This is obvious, due to interparticle voids filling by $CoFe_2O_4$ NP. Filling the voids by NP also leads to increasing contact points spots of CS particles, which lead to increase of mechanical properties of the material. Specimens series CS1-7.5 and CS2-7.5 (with 7.5 wt.% of $CoFe_2O_4$) in all CP and sintering temperature studied ranges characterises by higher compressive strength average for 30 MPa in comparison without $CoFe_2O_4$ addition. The overall tendency of the influence of the of CP on the compressive strength is the same as for CS without NP it is gradually in-crease.

Preprints (www.preprints.org) | NOT PEER-REVIEWED | Posted: 2 November 2023 doi:10.20944/preprints202311.0173.v1

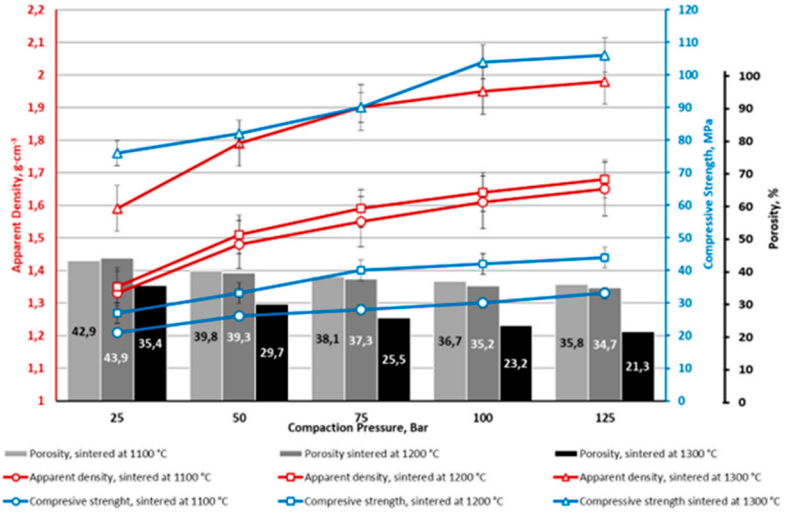

Figure 8. CS1-7.5 porous ceramics with 7.5 wt. % of $CoFe_2O_4$ apparent density, apparent porosity and compressive strength depending on CP and sintering temperature.

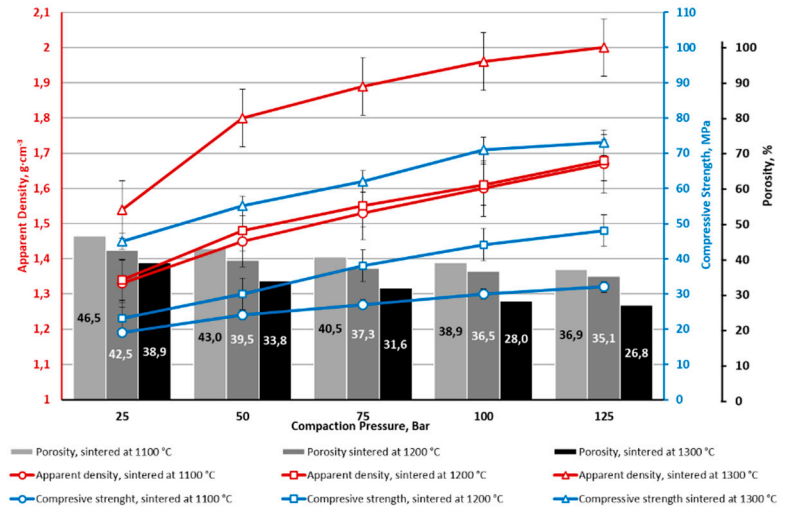

Figure 9. CS2-7.5 porous ceramics with 7.5 wt. % of $CoFe_2O_4$ apparent density, apparent porosity and compressive strength depending on CP and sintering temperature.

Similar regularities are also determined for materials with a ferrite content of 10 wt%. (Figures 10 and 11). Comparing the results obtained using cenospheres with a size of 150-250 μm (CS1) and 63-150 μm (CS2), it can be concluded that the size of the cenospheres does not significantly affect the sintering results – bulk density and apparent porosity. As known from [15], at temperatures above 1200 °C, cenospheres begin to plastically deform (Figure 6), which can explain the significant increase in sample density for samples sintered at 1300 °C, compared to samples sintered at temperatures of 1100 or 1200 °C. The plastic deformation leads to consolidation of the material by reduction of inter particle voids without the particle getting broken.

Preprints (www.preprints.org) | NOT PEER-REVIEWED | Posted: 2 November 2023 doi:10.20944/preprints202311.0173.v1

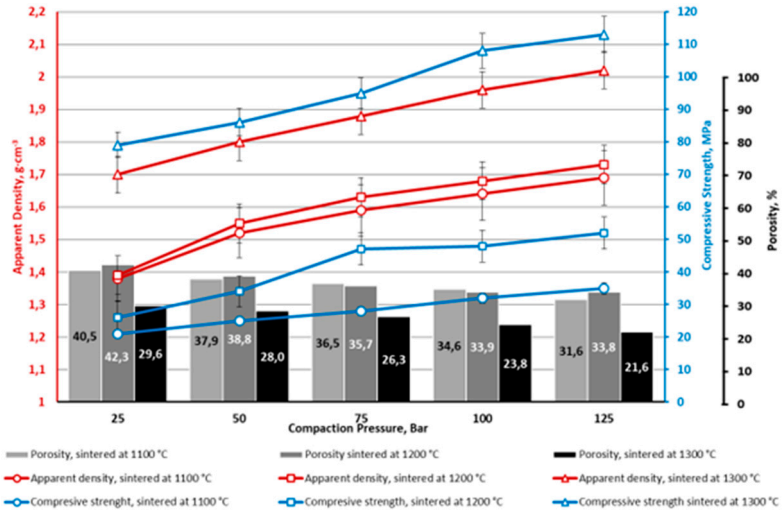

Figure 10. CS1-10 porous ceramics with 10 wt.% of $CoFe_2O_4$ bulk density, apparent porosity and compressive strength depending on CP and sintering temperature.

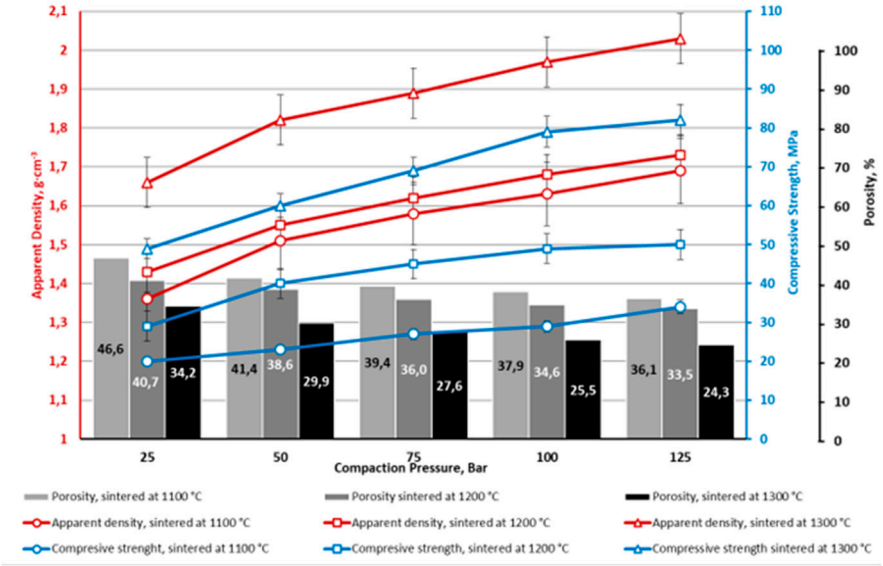

Figure 11. CS2-10 porous ceramics with 10 wt.% of $CoFe_2O_4$ bulk density, apparent porosity and compressive strength depending on CP and sintering temperature.

The nature of the samples with 20% ferrite additives (Figure 12) is similar to the samples with a smaller amount of ferrite additives: the density and compressive strength of the samples increase with the increase of pressing pressure and sintering temperature. Higher ferrite addition increases both material density and compressive strength.

Preprints (www.preprints.org) | NOT PEER-REVIEWED | Posted: 2 November 2023 doi:10.20944/preprints202311.0173.v1

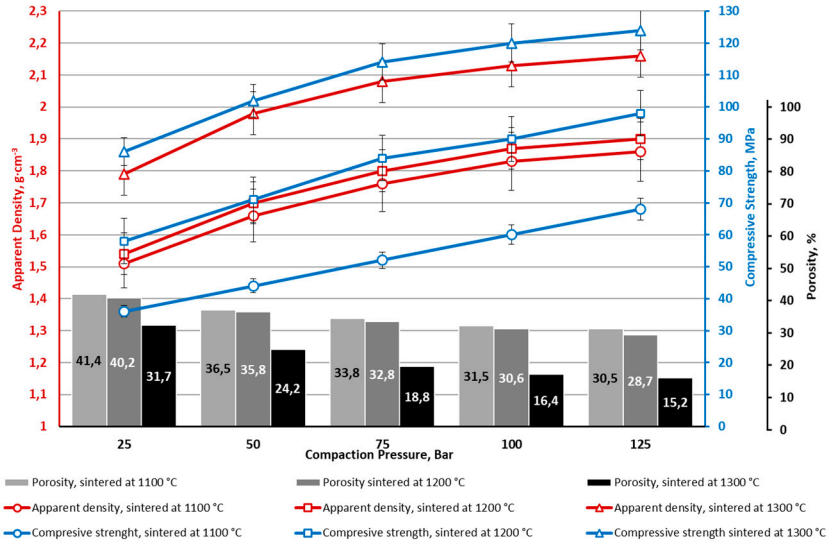

Figure 12. CS1-20 ceramics with 20 wt.% of $CoFe_2O_4$ bulk density, apparent porosity and compressive strength depending on CP and sintering temperature**.**

The relationship between ferrite NP content, CP, apparent density, and compressive strength for CS1 is shown in **Figure 13**. There is a clear relationship between the material's apparent density (red curves) and compressive strength (blue curves) and ferrite concentration - with the increase in ferrite concentration, the apparent density and compressive strength also increase. Apparent density and compressive strength increase monotonically as CP increases.

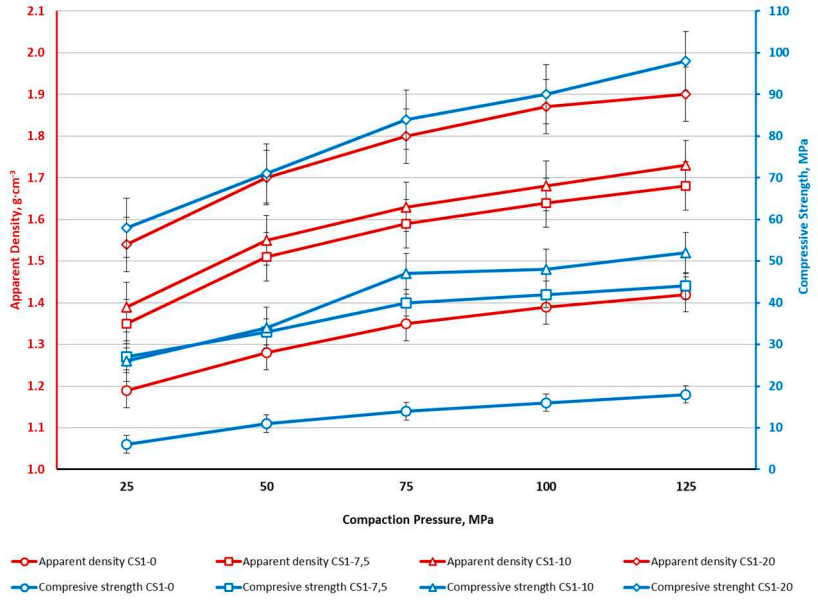

Figure 13. Effect of $CoFe_2O_4$ concentration on the apparent density and compressive strength of cenosphere CS1 ceramics (sintering temperature 1200 °C.

The relationship between ceramic apparent density (a), compressive strength (b) and CP and sintering temperature for CS1-7.5 and CS2 -7.5 is shown in Figure 14. As can be seen from Figure 14, the density of the samples grows monotonically with increasing com-paction pressure and does not depend on the size of the used cenospheres. In contrast to samples sintered at 1100 and 1200 °C, the density of samples sintered at 1300 °C is significantly higher, which could be related to the pronounced plastic deformation of ceno-spheres at this temperature. On the other hand, the

Preprints (www.preprints.org) | NOT PEER-REVIEWED | Posted: 2 November 2023 doi:10.20944/preprints202311.0173.v1

compressive strength of samples sintered at 1300 °C is significantly higher for CS1 (150-250 μm) samples than for CS2 samples.

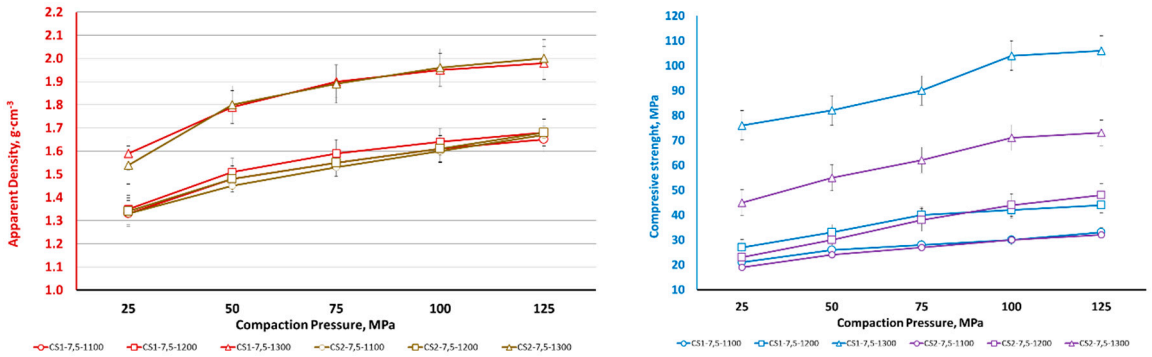

(**a**) (**b**)

Figure 14. Ceramic relative density (a) and compressive strength (b) depending on CP and sintering temperature for CS1-7.5 and CS2 -7.5.

Analysis of X-ray phases (**Figure 14**) shows that in the case of cenospheres and $CoFe_2O_4$ ceramics, their partial interaction takes place - mullite partially decomposes: Al_2O_3 enters the structure of $CoFe_2O_4$, while SiO_2 precipitates as a separate phase. The presence of the SiO_2 phase in sintered samples can also be partly explained by the crystallization of amorphous SiO_2 on the cenospheres.

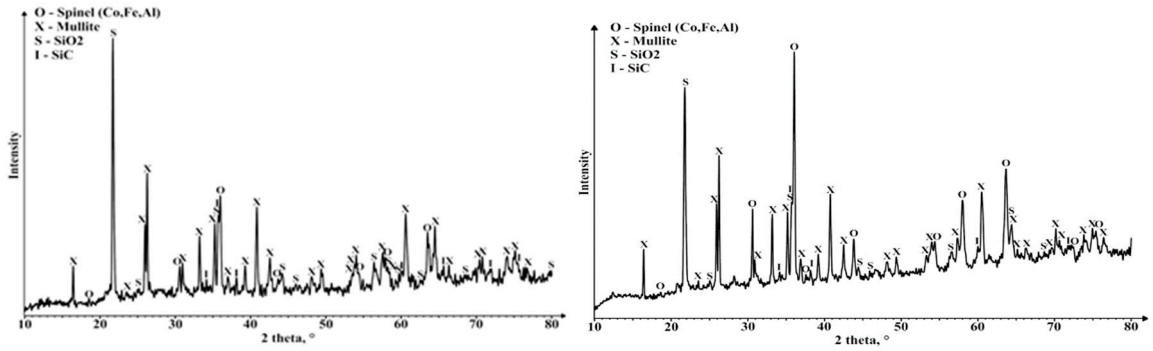

(a) **(b)**

Figure 14. Phase composition of ceramic (a) CS1–10 sintered at 1200 °C and (b) CS1-20 sintered at 1300 °C.

Scanning electron microscopy is used to study the structure of materials. To test the strength of the cenospheres, individual samples were pressed at a higher pressure (250 bars). SEM images (Figures 16 and 17) show that in the case of pure cenosphere ceramics, the ce-nospheres are either partially or fully crushed. The formation of mullite needles on the surface of the cenospheres can be observed in the SEM images of the sintered samples of cenospheres (CS1 and CS2) (Figure 16). At a CP of 250 bars, almost all spheres are destroyed (Figure 17). In well-sintered (1300 °C) CS1 samples at low CPs (25-50 bar), many cenospheres are intact (Figure 18).

Preprints (www.preprints.org) | NOT PEER-REVIEWED | Posted: 2 November 2023 doi:10.20944/preprints202311.0173.v1

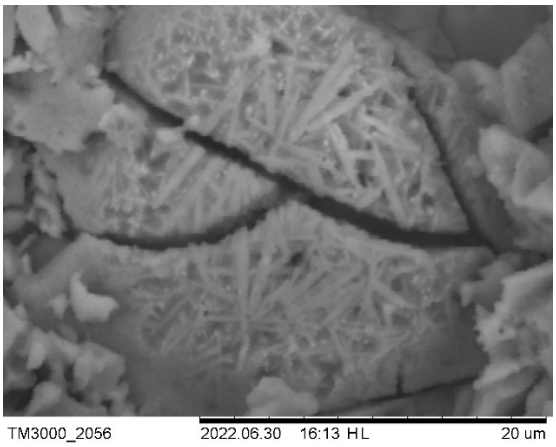

Figure 15. At a temperature of 1200 °C sintered CS1-0 cenospheres (CP 250 bar).

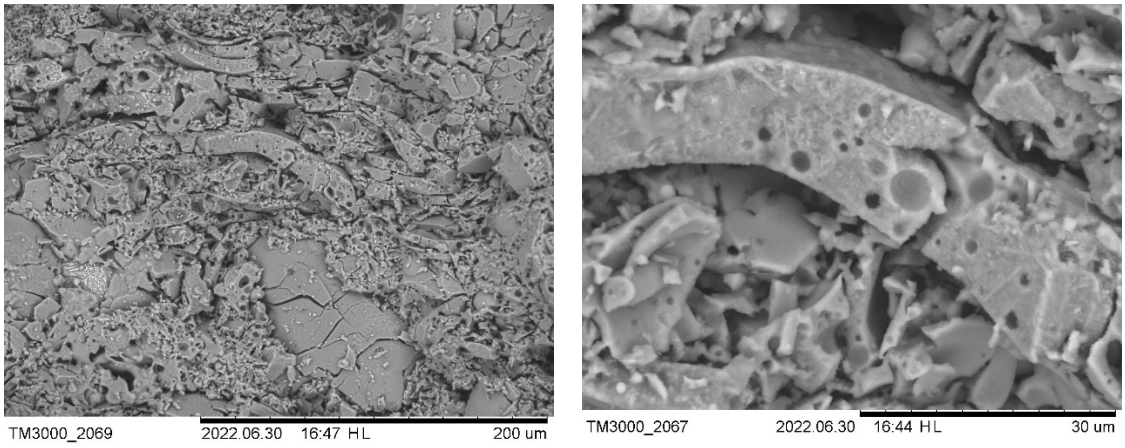

(**a**) (**b**)

Figure 16. At a temperature of 1200 °C sintered CS1-0 cenospheres (CP 250 bar).

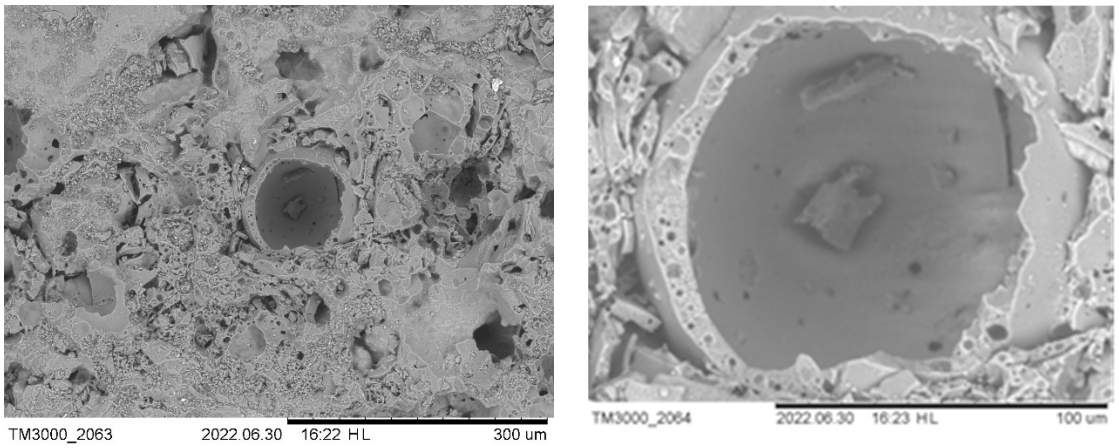

(**a**) (**b**)

Figure 17. At a temperature of 1300 °C sintered CS1-0 cenospheres (CP 25 bar).

The addition of $CoFe_2O_4$ improves sintering and mechanical strength, so the spheres are less crushed (Figure 19). In compositions of cenospheres with $CoFe_2O_4$, most of the spheres are healthy

Preprints (www.preprints.org) | NOT PEER-REVIEWED | Posted: 2 November 2023 doi:10.20944/preprints202311.0173.v1

(Figure 20. (the image was taken with an optical microscope)). Ferrite particles cover the cenospheres, thus increasing the density of the material and improving the mechanical properties

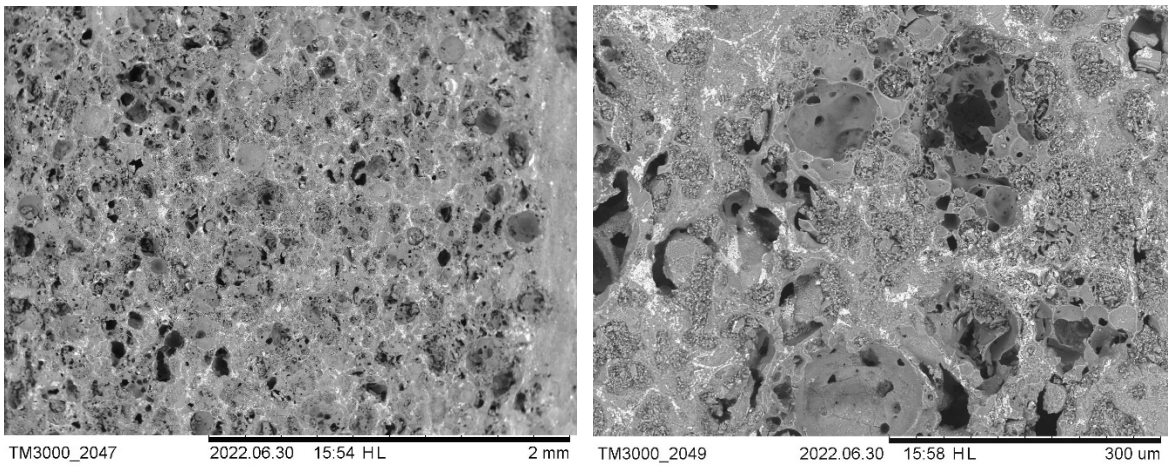

(**a**) (**b**)

Figure 18. Microstructure of ceramic CS1–20 sintered at 1300 °C (CP 25 bar).

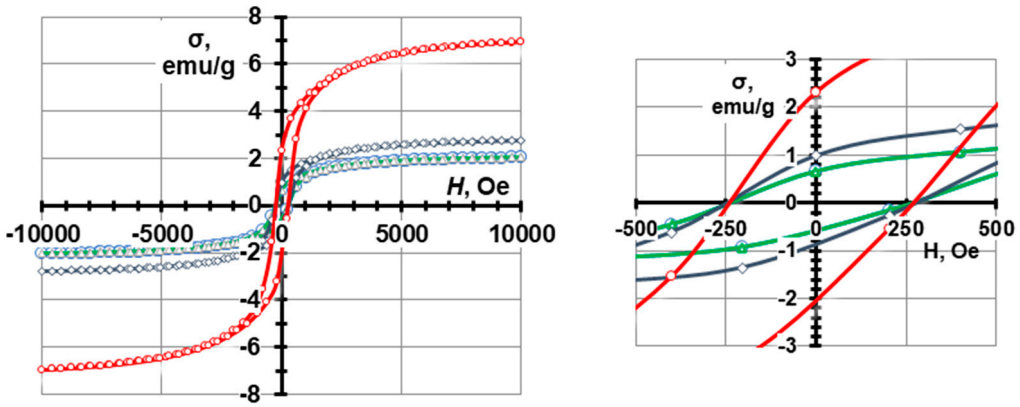

Figure 19. Magnetization hysteresis of CS1 nanocomposites with $CoFe_2O_4$ nanoparticles sintered at 1200 °C. $CoFe_2O_4$ = 7.5 (1), 10 (2), 20 (3).

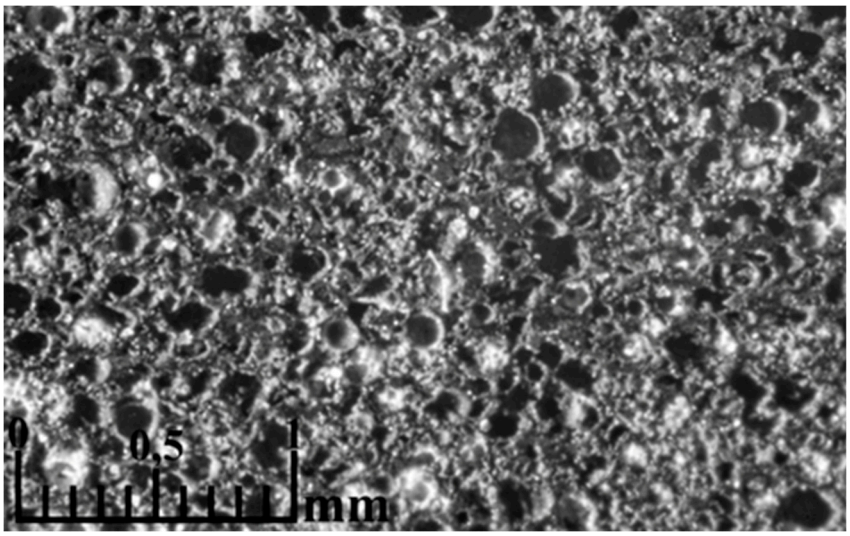

Figure 20. Microstructure of ceramic CS1 – 20 sintered at 1300 °C (CP 25 bar).

Preprints (www.preprints.org) | NOT PEER-REVIEWED | Posted: 2 November 2023 doi:10.20944/preprints202311.0173.v1

As a result of research, the optimal CP for samples of the given size is 25-75 bar.

The mechanical properties (compressive and bending strength) of some samples depending on CP, sintering temperature and concentration of ferrites are given in Table 2. For this purpose, plates 65x65x9 mm were made, from which samples were cut to determine compressive strength (10x10x9 mm) and bending strength (10x9x60 mm).

As can be seen from Table 2, a geometric factor can be observed - the density of cylindrical tablets obtained under the same conditions (temperature, CP) is higher than that of large plates. Compared to small-sized samples (in our case, the surface area of the small samples perpendicular to the compaction direction was 1 cm^2), the surface area of the plates exceeds 40 cm^2. Therefore, in a small volume, the material compresses more and the initial density at the same CP is higher.

Table 2. Density, compressive and bending strength of samples CS1 and CS2 with different content of CoFe2O4. Pressure 240 bar, sintered at 1300 °C.

Sample	Density, $g \cdot cm^{-3}$ (%)	Water absorption (W), %	Apparent porosity (π), %	Compressive strength ($\sigma_{comp.}$), MPa	Bending strength ($\sigma_{bend.}$)., MPa	Flexural modulus, MPa	Deformation (ε), %
CS1-0	1.03 (32.2)	50.7	52.0	12.4±0.1	7.1±0.4	1960±180	0.39
CS1-7.5	1.17 (35.0)	45.9	49.9	29.3±2.8	10.2±0.3	5190±130	0.41
CS1-10	1.31 (38.4)	33.7	44.2	47.4±12.6	17,9±1.6	4830±450	0.52
CS2-0	1.05 (32.8)	48.8	51.3	17.4±5.8	6.0±0.4	2690±310	0.21
CS2-10	1.32 (38.9)	34.2	45.1	41.7±6.2	12.3±1.9	5220±490	0.23

Figure 19 shows the hysteresis loop magnetization (σ) as a function of applied magnetic field (H) for the three CS1 samples sintered at 1200 °C. The values of saturation magnetization Ms, remanent magnetization Mr and coercivity Hc are listed in 3. The coercivity (H_c) of the ceramics with various ferrite content was 275 Oe. But as the ferrite content increases, the saturation magnetization (M_s) and remnant magnetization (M_r) of the ceramics also increase. The M_s value for ceramics with 7.5, 10, and 20 % ferrite was 6.93, 2.78, and 2.04 emu/g, respectively, and M_r values are 2.3, 1.0, and 0.65 Oe, respectively. It shows that the soft magnetic properties are improved with increasing ferrite content. Soft magnetism is indicative of low volume resistivity and better EMI shielding as observed in FeCoNi coated carbon fibers [48], and CI/Ti3C2Tx/PVDF multilayer structured composite films [49].

The coercivity of a material dictates its magnetization capacity. If it is high, the material stays magnetized for long and vice versa. For $CoFe_2O_4$ nanoparticles sintered at, the coercivity was reported to be 188.57 Oe at room temperature [50]. Compared to the pure $CoFe_2O_4$, the ceramic and ferrite material studied in this study had a higher value of coercivity of 275 Oe, which suggests that some hardening in the ferromagnetic properties of the material is detected. Although, it is important to note that while for CS1 ferrite, sintered at 1200 °C, the coercivity is the same, it is higher for CS2 at the same sintering temperature. Typically, it is the higher the coercivity of the materials does not.

The electromagnetic properties (saturation magnetization Ms, remanent magnetization Mr and coercivity Hc) of the material increase in direct proportion to the concentration of ferrite nanoparticles in the material (Table 3, Figures 21 and 22).

Table 3. Magnetic properties of CS1 and CS2 - CoFe2O4 ceramics, sintered at 1200 °C.

Sample	Magnetic properties		
	M_s, emu/g	M_r, emu/g	H_c, Oe
CS2 - 7.5 wt.% $CoFe_2O_4$	1.17	0.47	375
CS3 – 7.5 wt.% $CoFe_2O_4$	2.04	0.65	275
CS3 – 10 wt.% $CoFe_2O_4$	2.78	1.00	275
CS3 – 20 wt.% $CoFe_2O_4$	6.93	2.30	275

Preprints (www.preprints.org) | NOT PEER-REVIEWED | Posted: 2 November 2023 doi:10.20944/preprints202311.0173.v1

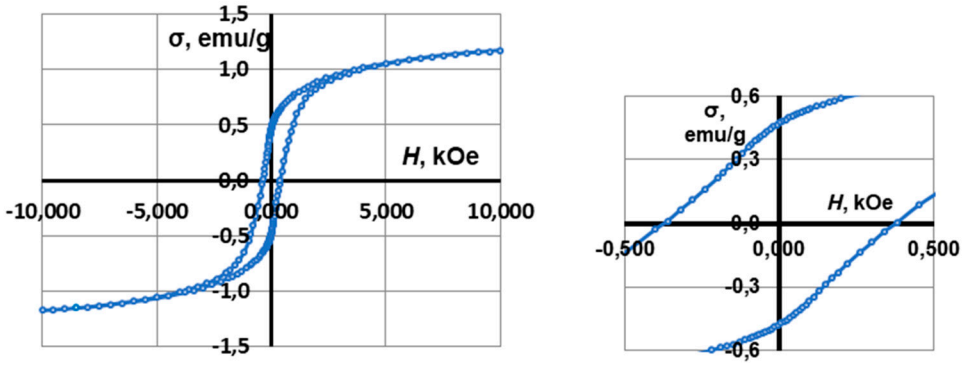

Figure 22. Magnetization hysteresis of CS2 nanocomposites with 7.5 wt.% $CoFe_2O_4$ nanoparicles sintered at 1200 °C.

Increasing the CP and sintering temperature contributes to the sintering of the material and the increase in mechanical strength, both in the case of pure cenosphere ceramics and in the composition with $CoFe_2O_4$. As SEM images show, in the case of pure cenosphere ceramics, the cenospheres are partially or completely destroyed, depending on the CP. Low CPs should be used to preserve the closed pore structure as much as possible. But then the mechanical strength of the material is not great. The addition of $CoFe_2O_4$ nanoparticles significantly improves the sinterability of ceramics even at low CPs, allowing to obtain highly porous ceramics with good mechanical strength. X-ray phase analysis (Figure 15.) shows that in the case of cenospheres - $CoFe_2O_4$ ceramics, there is a slight interaction between them - mullite partially decomposes: Al_2O_3 enters the structure of $CoFe_2O_4$, while SiO_2 precipitates as a separate phase.

The electromagnetic properties of the material are enhanced in direct proportion to the concentration of ferrite nanoparticles in the material.

4. Conclusions

Lightweight high-temperature ceramics material with an ferromagnetic shielding effect were obtained by conventional pressure-sintering method using cenosphere and $CoFe_2O_4$ nanoparticles. Additives of ferrite nanoparticles improve the sintering of cenospheres, increasing the density of the material and increasing the mechanical properties. The porous structure of the samples largely depends on the CP of the samples: at CPs of 25-75 bars, whole cenospheres are largely preserved in the sample; at higher CPs, there is significant crushing of cenospheres, a decrease in porosity and an increase in density. Depending on the sample CP and sintering temperature, samples with a density of 1.2-2.1 g/cm^3 and a compressive strength of 1.5-125.0 MPa were obtained. The bending strength of the obtained samples is determined within 10 - 20 MPa. The magnetic properties of the samples change in proportion to the amount of $CoFe_2O_4$ in the sample.

Author Contributions: Conceptualization, A.S., J.B. and I.Z.; methodology, I.Z., J.B.; investigation, I.Z., V.A., M.M. and A.S.; resources A.S. and I.Z.; data curation, V.A. and A.S.; writing—original draft preparation, I.Z., A.S., V.A., J.B. and A.K.S.; writing—review and editing, A.S. and A.K.S.; visualisation, V.A., I.Z. and V.A.; supervision, A.S and I.Z.; project administration, A.S.; funding acquisition, A.S. All authors have read and agreed to the published version of the manuscript.

Funding: This research was funded by VPP AIPP project Nr. VPP-AIPP-2021/1-0015 "Combined lightweight, high-temperature resistant hybrid composite for combined protection of drones from Direct Energy Weapon". The article was published with the financial support from the Riga Technical University Research Support Fund.

Conflicts of Interest: The authors declare no conflict of interest.

References

1. Markham, D. Shielding: Quantifying the Shielding Requirements for Portable Electronic Design and Providing New Solutions by Using a Combination of Materials and Design. *Mater Des* **1999**, *21*, doi:10.1016/s0261-3069(99)00049-7.
2. Lundgren, U.; Ekman, J.; Delsing, J. Shielding Effectiveness Data on Commercial Thermoplastic Materials. *IEEE Trans Electromagn Compat* **2006**, *48*, doi:10.1109/TEMC.2006.879352.
3. Huang, J. -C EMI Shielding Plastics: A Review. *Advances in Polymer Technology* **1995**, *14*, doi:10.1002/adv.1995.060140205.
4. Zhang, L.; Wang, L.B.; See, K.Y.; Ma, J. Effect of Carbon Nanofiber Reinforcement on Electromagnetic Interference Shielding Effectiveness of Syntactic Foam. *J Mater Sci* **2013**, *48*, doi:10.1007/s10853-013-7597-x.
5. Ameli, A.; Jung, P.U.; Park, C.B. Through-Plane Electrical Conductivity of Injection-Molded Polypropylene/Carbon-Fiber Composite Foams. *Compos Sci Technol* **2013**, *76*, doi:10.1016/j.compscitech.2012.12.008.
6. Han, D.; Mei, H.; Xiao, S.; Xue, W.; Bai, Q.; Cheng, L. CNT/SiC Composites Produced by Direct Matrix Infiltration of Self-Assembled CNT Sponges. *J Mater Sci* **2017**, *52*, doi:10.1007/s10853-017-1096-4.
7. Zhang, H. Bin; Yan, Q.; Zheng, W.G.; He, Z.; Yu, Z.Z. Tough Graphene-Polymer Microcellular Foams for Electromagnetic Interference Shielding. *ACS Appl Mater Interfaces* **2011**, *3*, doi:10.1021/am200021v.
8. Xia, X.; Mazzeo, A.D.; Zhong, Z.; Weng, G.J. An X-Band Theory of Electromagnetic Interference Shielding for Graphene-Polymer Nanocomposites. *J Appl Phys* **2017**, *122*, doi:10.1063/1.4992074.
9. Zhao, H.B.; Fu, Z.B.; Chen, H.B.; Zhong, M.L.; Wang, C.Y. Excellent Electromagnetic Absorption Capability of Ni/Carbon Based Conductive and Magnetic Foams Synthesized via a Green One Pot Route. *ACS Appl Mater Interfaces* **2016**, *8*, doi:10.1021/acsami.5b10805.
10. Zeng, Z.; Chen, M.; Pei, Y.; Seyed Shahabadi, S.I.; Che, B.; Wang, P.; Lu, X. Ultralight and Flexible Polyurethane/Silver Nanowire Nanocomposites with Unidirectional Pores for Highly Effective Electromagnetic Shielding. *ACS Appl Mater Interfaces* **2017**, *9*, doi:10.1021/acsami.7b07643.
11. Gupta, N.; Zeltmann, S.E.; Shunmugasamy, V.C.; Pinisetty, D. Applications of Polymer Matrix Syntactic Foams. *JOM* **2014**, *66*, doi:10.1007/s11837-013-0796-8.
12. Strzałkowska, E.; Adamczyk, Z. Influence of Chemical Composition of Fly-Ash Cenospheres on Their Grains Size. *International Journal of Environmental Science and Technology* **2020**, *17*, 809–818, doi:10.1007/s13762-019-02512-2.
13. Choo, T.F.; Salleh, M.A.M.; Kok, K.Y.; Matori, K.A.; Rashid, S.A. Effect of Temperature on Morphology, Phase Transformations and Thermal Expansions of Coal Fly Ash Cenospheres. *Crystals (Basel)* **2020**, *10*, 1–11, doi:10.3390/cryst10060481.
14. Adesina, A. Sustainable Application of Cenospheres in Cementitious Materials – Overview of Performance. *Developments in the Built Environment* 2020, *4*.
15. Shishkin, A.; Abramovskis, V.; Zalite, I.; Singh, A.K.; Mezinskis, G.; Popov, V.; Ozolins, J. Physical, Thermal, and Chemical Properties of Fly Ash Cenospheres Obtained from Different Sources. *Materials* **2023**, *16*, doi:10.3390/ma16052035.
16. Ranjbar, N.; Kuenzel, C. Cenospheres: A Review. *Fuel* 2017, *207*, 1–12.
17. Baronins, J.; Setina, J.; Sahmenko, G.; Lagzdina, S.; Shishkin, A. Pore Distribution and Water Uptake in a Cenosphere-Cement Paste Composite Material. In Proceedings of the IOP Conference Series: Materials Science and Engineering; 2015; Vol. 96.
18. Shishkin, A.; Drozdova, M.; Kozlov, V.; Hussainova, I.; Lehmhus, D. Vibration-Assisted Sputter Coating of Cenospheres: A New Approach for Realizing Cu-Based Metal Matrix Syntactic Foams. *Metals (Basel)* **2017**, *7*, doi:10.3390/met7010016.
19. Luong, D.; Lehmhus, D.; Gupta, N.; Weise, J.; Bayoumi, M. Structure and Compressive Properties of Invar-Cenosphere Syntactic Foams. *Materials* **2016**, *9*, doi:10.3390/ma9020115.
20. Kasar, A.K.; Gupta, N.; Rohatgi, P.K.; Menezes, P.L. A Brief Review of Fly Ash as Reinforcement for Composites with Improved Mechanical and Tribological Properties. *JOM* 2020, *72*, 2340–2351.
21. Doddamani, M.; Gupta, N. 3D Printing of Fly Ash-Based Syntactic Foams. In *Handbook of Fly Ash*; 2021.
22. Zalite, I.; Heidemane, G.; Grabis, J.; Maiorov, M. The Synthesis and Characterization of Nickel and Cobalt Ferrite Nanopowders Obtained by Different Methods. In *Powder Technology*; 2018.
23. Jauhar, S.; Kaur, J.; Goyal, A.; Singhal, S. Tuning the Properties of Cobalt Ferrite: A Road towards Diverse Applications. *RSC Adv* 2016, *6*.
24. Chakradhary, V.K.; Ansari, A.; Akhtar, M.J. Design, Synthesis, and Testing of High Coercivity Cobalt Doped Nickel Ferrite Nanoparticles for Magnetic Applications. *J Magn Magn Mater* **2019**, *469*, doi:10.1016/j.jmmm.2018.09.021.
25. Gul, I.H.; Ahmed, W.; Maqsood, A. Electrical and Magnetic Characterization of Nanocrystalline Ni-Zn Ferrite Synthesis by Co-Precipitation Route. *J Magn Magn Mater* **2008**, *320*, doi:10.1016/j.jmmm.2007.05.032.

26. Pubby, K.; Meena, S.S.; Yusuf, S.M.; Bindra Narang, S. Cobalt Substituted Nickel Ferrites via Pechini's Sol–Gel Citrate Route: X-Band Electromagnetic Characterization. *J Magn Magn Mater* **2018**, *466*, doi:10.1016/j.jmmm.2018.07.038.
27. Sagayaraj, R.; Aravazhi, S.; Chandrasekaran, G. Review on Structural and Magnetic Properties of (Co–Zn) Ferrite Nanoparticles. *Int Nano Lett* **2021**, doi:10.1007/s40089-021-00343-z.
28. Dippong, T.; Levei, E.A.; Cadar, O. Recent Advances in Synthesis and Applications of MFe2O4 (M = Co, Cu, Mn, Ni, Zn) Nanoparticles. *Nanomaterials* 2021, *11*.
29. Wang, M.; Zhang, Y.; Dong, C.; Chen, G.; Guan, H. Preparation and Electromagnetic Shielding Effectiveness of Cobalt Ferrite Nanoparticles/Carbon Nanotubes Composites. *Nanomaterials and Nanotechnology* **2019**, *9*, doi:10.1177/1847980419837821.
30. Soleimani, H.; Yusuf, J.Y.; Chuan, L.K.; Soleimani, H.; bin Sabar, M.L.; Öchsner, A.; Abbas, Z.; Balogun, A.I.; Kozlowski, G. In-Situ Preparation of CoFe2O4 Nanoparticles on Eggshell Membrane-Activated Carbon for Microwave Absorption. *Heliyon* **2023**, *9*, doi:10.1016/j.heliyon.2023.e13256.
31. Molaei, S.; Ghadermazi, M. Copper-Decorated Core–Shell Structured Ordered Mesoporous Containing Cobalt Ferrite Nanoparticles as High-Performance Heterogeneous Catalyst toward Synthesis of Tetrazole. *Sci Rep* **2023**, *13*, doi:10.1038/s41598-023-42094-1.
32. Lopez-Santiago, A.; Grant, H.R.; Gangopadhyay, P.; Voorakaranam, R.; Norwood, R.A.; Peyghambarian, N. Cobalt Ferrite Nanoparticles Polymer Composites Based All-Optical Magnetometer. *Opt Mater Express* **2012**, *2*, doi:10.1364/ome.2.000978.
33. El-Masry, M.M.; Ramadan, R.; Ahmed, M.K. The Effect of Adding Cobalt Ferrite Nanoparticles on the Mechanical Properties of Epoxy Resin. *Results in Materials* **2020**, *8*, doi:10.1016/j.rinma.2020.100160.
34. Endrodi, B.; Hursán, D.; Petrilla, L.; Bencsik, G.; Visy, C.; Chams, A.; Maslah, N.; Perruchot, C.; Jouini, M. Incorporation of Cobalt-Ferrite Nanoparticles into a Conducting Polymer in Aqueous Micellar Medium: Strategy to Get Photocatalytic Composites. *Acta Chim Slov* **2014**, *61*.
35. Kumar, Y.; Sharma, A.; Shirage, P.M. Shape-Controlled CoFe2O4 Nanoparticles as an Excellent Material for Humidity Sensing. *RSC Adv* **2017**, *7*, doi:10.1039/c7ra11072c.
36. Nam, P.H.; Lu, L.T.; Linh, P.H.; Manh, D.H.; Thanh Tam, L.T.; Phuc, N.X.; Phong, P.T.; Lee, I.J. Polymer-Coated Cobalt Ferrite Nanoparticles: Synthesis, Characterization, and Toxicity for Hyperthermia Applications. *New Journal of Chemistry* **2018**, *42*, doi:10.1039/c8nj01701h.
37. Nikitin, A.A.; Arkhipov, V.A.; Chmelyuk, N.S.; Ivanova, A. V; Vodopyanov, S.S.; Garanina, A.S.; Soldatov, M.A.; Gritsai, M.A.; Cherepanov, V.M.; Barbotina, N.N.; et al. *Supporting Information Multifunctional Anisotropic Rod-Shaped CoFe2O4 Nanoparticles for Magnetic Resonance Imaging and Magneto-Mechanical Therapy FeOOH 2q (Degree) (130) FeOOH 2q (Degree) (130) (240)*;
38. Caldeira, L.E.; Guaglianoni, W.C.; Venturini, J.; Arcaro, S.; Bergmann, C.P.; Bragança, S.R. Sintering-Dependent Mechanical and Magnetic Properties of Spinel Cobalt Ferrite (CoFe2O4) Ceramics Prepared via Sol-Gel Synthesis. *Ceram Int* **2020**, *46*, doi:10.1016/j.ceramint.2019.09.240.
39. Zhou, J.; Tan, R.; Yao, Z.; Lin, H.; Li, Z. Preparation of CoFe2O4 Hollow Spheres with Carbon Sphere Templates and Their Wave Absorption Performance. *Mater Chem Phys* **2020**, *244*, doi:10.1016/j.matchemphys.2020.122697.
40. Liu, Y.; Chen, Z.; Zhang, Y.; Feng, R.; Chen, X.; Xiong, C.; Dong, L. Broadband and Lightweight Microwave Absorber Constructed by in Situ Growth of Hierarchical CoFe2O4/Reduced Graphene Oxide Porous Nanocomposites. *ACS Appl Mater Interfaces* **2018**, *10*, doi:10.1021/acsami.8b02137.
41. Singh, A.K.; Shishkin, A.; Koppel, T.; Gupta, N. Porous Materials for EMI Shielding. In *Materials for Potential EMI Shielding Applications Processing, Properties and Current Trends*; Kuruvilla, J., Runcy, W., Gejo, G., Eds.; Elsevier B.V.: Amsterdam, 2019; pp. 287–314 ISBN 978-0-12-817590-3.
42. Yadav, R.S.; Anju; Jamatia, T.; Kuřitka, I.; Vilčáková, J.; Škoda, D.; Urbánek, P.; Machovský, M.; Masař, M.; Urbánek, M.; et al. Excellent, Lightweight and Flexible Electromagnetic Interference Shielding Nanocomposites Based on Polypropylene with MnFe2O4 Spinel Ferrite Nanoparticles and Reduced Graphene Oxide. *Nanomaterials* **2020**, *10*, doi:10.3390/nano10122481.
43. Gao, Y.; Wang, Z. Microwave Absorption and Electromagnetic Interference Shielding Properties of Li-Zn Ferrite-Carbon Nanotubes Composite. *J Magn Magn Mater* **2021**, *528*, doi:10.1016/j.jmmm.2021.167808.
44. Phan, C.H.; Mariatti, M.; Koh, Y.H. Electromagnetic Interference Shielding Performance of Epoxy Composites Filled with Multiwalled Carbon Nanotubes/Manganese Zinc Ferrite Hybrid Fillers. *J Magn Magn Mater* **2016**, *401*, doi:10.1016/j.jmmm.2015.10.067.
45. Zalite, I.; Heidemane, G.; Kodols, M.; Grabis, J.; Maiorov, M. The Synthesis, Characterization and Sintering of Nickel and Cobalt Ferrite Nanopowders. *Medziagotyra* **2012**, *18*, doi:10.5755/j01.ms.18.1.1332.
46. Liu, H.Y.; Li, Y.S. Synthesis and Microwave Absorbing Properties of Cobalt Ferrite. In Proceedings of the IOP Conference Series: Materials Science and Engineering; 2018; Vol. 292.
47. Zalite, I.; Heidemane, G.; Krumiņa, A.; Rašmane, D.; Grabis, J.; Maiorov, M. Characteristics of Sintered Materials Obtained from Ferrite Nanopowders Synthesised with Different Methods. In Proceedings of the Key Engineering Materials; 2018; Vol. 762.

48. Yim, Y.J.; Lee, J.J.; Tugirumubano, A.; Go, S.H.; Kim, H.G.; Kwac, L.K. Electromagnetic Interference Shielding Behavior of Magnetic Carbon Fibers Prepared by Electroless Feconi-Plating. *Materials* **2021**, *14*, doi:10.3390/ma14143774.
49. Liu, Q.; Zhang, Y.; Liu, Y.; Li, C.; Liu, Z.; Zhang, B.; Zhang, Q. Magnetic Field-Induced Strategy for Synergistic CI/Ti3C2Tx/PVDF Multilayer Structured Composite Films with Excellent Electromagnetic Interference Shielding Performance. *J Mater Sci Technol* **2022**, *110*, doi:10.1016/j.jmst.2021.06.084.
50. Ali, S.A.; Matin, M.A.; Hakim, M.A.; Islam, M.F. Effects of CoFe2O4 Substitution on Magnetic Properties of NiFe2O4 Spinel Ferrite. In Proceedings of the IOP Conference Series: Materials Science and Engineering; 2018; Vol. 438.